Published in final edited form as:

*ACS Biomater Sci Eng*. 2020 March 09; 6(3): 1321–1332. doi:10.1021/acsbiomaterials.9b01487.

# Coating Topologically Complex Electrospun Fibers with Nanothin Silk Fibroin Enhances Neurite Outgrowth in Vitro

**Alexis M. Ziemba**,
Department of Biomedical Engineering and Center for Biotechnology and Interdisciplinary Sciences, Rensselaer Polytechnic Institute, Troy, New York 12180, United States;

**Tanner D. Fink**,
Department of Chemical and Biological Engineering and Center for Biotechnology and Interdisciplinary Sciences, Rensselaer Polytechnic Institute, Troy, New York 12180, United States

**Mary Clare Crochiere**,
Department of Biomedical Engineering and Center for Biotechnology and Interdisciplinary Sciences, Rensselaer Polytechnic Institute, Troy, New York 12180, United States

**Devan L. Puhl**,
Department of Biomedical Engineering and Center for Biotechnology and Interdisciplinary Sciences, Rensselaer Polytechnic Institute, Troy, New York 12180, United States;

**Samichya Sapkota**,
Department of Biomedical Engineering and Center for Biotechnology and Interdisciplinary Sciences, Rensselaer Polytechnic Institute, Troy, New York 12180, United States

**Ryan J. Gilbert***,
Department of Biomedical Engineering and Center for Biotechnology and Interdisciplinary Sciences, Rensselaer Polytechnic Institute, Troy, New York 12180, United States;

**R. Helen Zha***

**Corresponding Authors: Ryan J. Gilbert** – Department of Biomedical Engineering and Center for Biotechnology and Interdisciplinary Sciences, Rensselaer Polytechnic Institute, Troy, New York 12180, United States; gilber2@rpi.edu, **R. Helen Zha** – Department of Chemical and Biological Engineering and Center for Biotechnology and Interdisciplinary Sciences, Rensselaer Polytechnic Institute, Troy, New York 12180, United States; zhar@rpi.edu.

Author Contributions

A.M.Z., T.D.F., and M.C.C. made equal design, experimental, and writing contributions to the manuscript. A.M.Z., T.D.F., and M.C.C. contributed equally to this manuscript and did the primary planning of this study. A.M.Z. and T.D.F. wrote the manuscript with contributions from M.C.C. D.L.P. fabricated fibers. S.S. analyzed fiber morphology characteristics. T.D.F. conducted the silk coating procedure, contact angle testing, $\zeta$-potential experiments, FITC-tagging, and FTIR. A.M.Z. and M.C.C. conducted DRG and astrocyte experiments and all fluorescence microscopy-related experiments. A.M.Z. did all statistical analyses. R.H.Z. and R.J.G. edited the manuscript. A.M.Z., T.D.F., M.C.C., D.L.P., S.S., R.H.Z., and R.J.G. discussed experimental work and have reviewed and have given approval to the final version of the manuscript.

Complete contact information is available at: https://pubs.acs.org/10.1021/acsbiomaterials.9b01487

Supporting Information

The Supporting Information is available free of charge at https://pubs.acs.org/doi/10.1021/acsbiomaterials.9b01487.
Materials and equipment information, Congo Red staining, complete FITC tagging images, ellipsometry and SEM of silk-coated fibers, sample DRG images, pilot astrocyte data, and complete statistical analyses (PDF)

Any opinions, findings, and conclusions or recommendations expressed in this material are those of the authors and do not necessarily reflect the views of the National Science Foundation.

The authors declare no competing financial interest.

Department of Chemical and Biological Engineering and Center for Biotechnology and Interdisciplinary Sciences, Rensselaer Polytechnic Institute, Troy, New York 12180, United States;

## Abstract

Electrospun poly-L-lactic acid (PLLA) fibers are commonly used for tissue engineering applications because of their uniform morphology, and their efficacy can be further enhanced via surface modification. In this study, we aimed to increase neurite outgrowth along electrospun fibers by coating with silk fibroin (SF), a bioinert protein derived from *Bombyx mori* cocoon threads, shown to be neurocompatible. Aligned PLLA fibers were electrospun with smooth, pitted, and divoted surface nanotopographies and coated with SF by immersion in coating solution for either 12 or 24 h. Specifically, thin-film coatings of SF were generated by leveraging the controlled self-assembly of SF in aqueous conditions that promote $\beta$-sheet assembly. For both 12- and 24-h coatings, Congo Red staining for $\beta$-sheet structures confirmed the presence of SF coatings on PLLA fibers. Confocal imaging of fluorescein-labeled SF further demonstrated a homogeneous coating formation on PLLA fibers. No change in the water contact angle of the surfaces was observed after coating; however, an increase in the isoelectric point (pI) to values comparable with the theoretical pI of SF was seen. Notably, there was a significant trend of increased dorsal root ganglia (DRG) adhesion on scaffolds coated with SF, as well as greater neurite outgrowth on pitted and divoted fibers that had been coated with SF. Ultimately, this work demonstrated that thin-film SF coatings formed by self-assembly uniformly coat electrospun fibers, providing a new strategy to increase the neuroregenerative capacity of electrospun scaffolds. To our knowledge, this is the first instance of biomedical modification of topologically complex substrates using noncovalent methods.

## Graphical Abstract

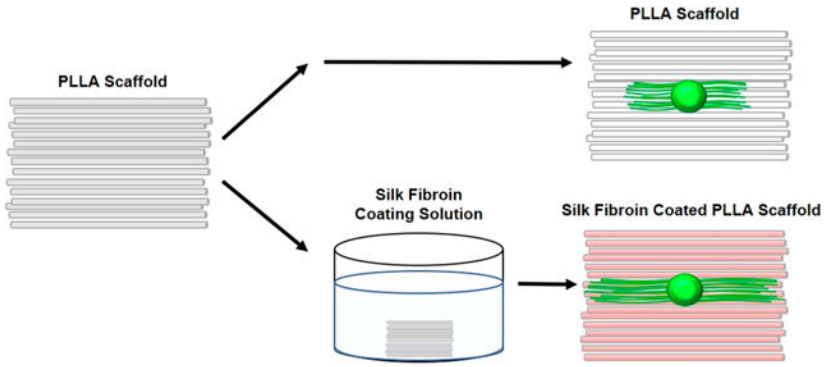


### Keywords

electrospun fiber; poly-L-lactic acid; silk fibroin; dorsal root ganglia; neurite outgrowth

## INTRODUCTION

Aligned electrospun fibers promote axonal regeneration, following peripheral nerve[1,2] and spinal cord injury[3,4] in preclinical models. Poly-L-lactic acid (PLLA) is commonly used for

neural applications because it is an FDA-approved biodegradable material that produces highly aligned and uniform fibers.[3,5] PLLA scaffolds also exhibit tensile properties that remain constant over the course of months,[6] which is of appropriate duration for neural injury repair that takes months to years to recover lost sensory and motor functions. As studies have demonstrated neurites extend better on topological substrates,[7] our group has fabricated electrospun fibers with three different types of surface nanotopography and assessed neuron, astrocyte, and macrophage responses in vitro.[8–11] Smooth fibers have a smooth surface with no nanotopography, so cells only sense the curvature of each fiber. Pitted fibers have holes ranging from ~50 to 200 nm in length, resulting in a larger fiber specific surface area ($m^2/g$)[10] for which cells can interact. Finally, divoted fibers have shallow cavities that are parallel to the length of each fiber. We previously assessed the dorsal root ganglia (DRG) response to PLLA fibers with various surface topologies; individual DRG neurons had increased branching on laminin coated PLLA fibers with pits and divots.[10] Even with the laminin coating, the neurons still sensed the surface nanotopography and extended more neurites than on surfaces without topography. While these PLLA fibers have desirable characteristics for neural regeneration, the PLLA surface is hydrophobic[12] and lacks cell attachment sites to stimulate neurite extension. Thus, electrospun PLLA fibers with increased surface topography may be more efficacious when combined with a thin, bioactive coating that enhances neural cell adhesion and stimulates more robust neurite extension.

Silk fibroin (SF) is a fibrous protein extracted from the cocoons of domesticated *Bombyx mori* silkworm. Materials made from SF, such as fibers, hydrogels, porous sponges, films, and nonwoven mats, have gained much attention in the recent decade for biomedical applications.[9,10] In particular, SF generally elicits a lower inflammatory response than polymers, such as collagen and polylactic acid,[13] and the mechanical properties[14] and degradation rates[15] of silk-based materials can be augmented by varying the degree of silk I (less crystalline) or silk II (crystalline) structures in the material by post-treatment methods.[16] While in vivo degradation rates will depend on a variety of factors, such as morphology, degree of silk I and silk II structures in the material, and location in the body, SF fibers can persist for several months in vivo after implantation.[16,17] With regards to neuronal regeneration applications, studies have confirmed the biocompatibility of SF with neurons by seeding DRG[18,19] and hippocampal neurons onto SF substrates[20] without any cytotoxic effects. Qu et al. analyzed neurite outgrowth on electrospun SF scaffolds with 400, 800, and 1200 nm diameter fibers and found that the 400 nm fibers provided the greatest support for the development and maturation of cortical neurons.[21] Wang et al. studied the response of human embryonic stem cells to electrospun SF scaffolds with 400 and 800 nm diameter fibers and also found that aligned 400 nm diameter fibers lead to increased viability, neuronal differentiation, and neurite outgrowth.[22] Studies have also encapsulated nerve growth factor in SF/poly(lactic acid) fibers, and when plasma treated, the fibers supported significant elongation of neurites and differentiation of PC12 cells.[23] Taken together, these results demonstrate the promise of SF scaffolds in treating nervous system injury and suggest that applying SF to PLLA scaffolds may enhance their regenerative efficacy.

Previous studies have demonstrated successful fabrication of electrospun silk scaffolds.[24–26] Despite the potential benefits of silk scaffolds and fibers for neural regeneration, there are no

examples in literature of highly aligned electrospun SF fibers without additives, such as poly(ethylene oxide).[27] Electrospun SF scaffolds with lower levels of fiber alignment have been fabricated;[28,29] however, these are not optimal for the regeneration of aligned nerve tracts. Furthermore, electrospun silk fibers require post-treatment with methanol or water-annealing to fabricate stable, insoluble fibers with high $\beta$-sheet content.[30] These restrictions limit the potential of electrospun SF scaffolds to guide axonal extension longitudinally and to incorporate bioactive components into the scaffold. An alternative to directly electrospinning SF is to coat SF onto prefabricated, highly aligned electrospun scaffolds made from biocompatible synthetic polymers with desired mechanical properties. A conformal and thin layer of SF is desirable over a thick and heterogeneous coating to maintain desired surface features such as fiber diameter and surface nanotopography.

Recently, Zha et al. demonstrated that nanothin coatings can be formed on a variety of surfaces by controlling the nonspecific adsorption and self-assembly of recombinant spider silk eADF4(C16). Results showed that spider silk coatings were smooth, homogeneous, and stable to prolonged incubation in aqueous environments.[31] Materials are coated in aqueous solution with phosphate ions added as a kosmotropic agent to induce intermolecular $\beta$-sheet formation and is thus highly compatible with biomaterials applications. This noncovalent coating process is tolerant of hydrophobic, as well as hydrophilic, substrates without requiring special surface chemistries, activating pretreatments, or covalent cross-linking. However, eADF4(C16) films have shown low adhesion and lack of proliferation of BALB/3T3 mouse fibroblasts.[32] Thus, to enhance neuron adhesion and neurite extension through surface modification of prefabricated scaffolds, while preserving scaffold topologies, this coating strategy could be applied with other silk proteins that exhibit more favorable biomedical properties.

Therefore, this study aimed to use self-assembled *B. mori* SF coatings to improve the neuroregenerative efficacy of aligned electrospun PLLA fibers. This strategy combines the long-term stability and cost-effectiveness of PLLA fibers with the enhanced biocompatibility of SF. This unique coating strategy produces nanolayers that maintain fiber topography, which is essential to direct neurite outgrowth. We hypothesized that the silk coating would increase fiber surface wettability and ultimately enhance neurite extension from DRG. To test this, three different fiber types were electrospun: (1) fibers without nanotopography (smooth fibers), (2) fibers with pitted nanotopography, and (3) fibers with divoted nanotopography and were coated with SF for 12 or 24 h. Fiber surface morphology was characterized using scanning electron microscopy (SEM). Surface wettability and charge differences between uncoated and SF-coated fibers were assessed via contact angle goniometry and $\zeta$-potential, respectively. The presence of SF coating was also confirmed using Congo Red staining, FITC tagging, and SEM. DRG adhesion and neurite outgrowth were assessed on uncoated and SF-coated PLLA scaffolds with varying surface nanotopography using immunocytochemistry and confocal microscopy. Ultimately, we demonstrate that SF coatings form homogeneously on electrospun PLLA fibers, resulting in measurable changes in surface chemistry without significantly altering fiber topography. These coated PLLA scaffolds showed significantly improved neurite adhesion and extension, demonstrating the first instance of SF self-assembly as a method for biomedical modification of topologically complex substrates.

## METHODS

All materials and equipment information are displayed in Tables S1 and S2.

### Electrospinning.

Electrospun fiber scaffolds with varying surface nanotopography (smooth, pitted, and divoted) were fabricated using previously described techniques.[33] Briefly, poly-L-lactic acid (PLLA) was magnetically stirred in chloroform ($CHCl_3$) for approximately 2 h. Following PLLA dissolution, PLLA scaffolds with smooth, pitted, and divoted surface nanotopography were produced using the parameters listed in Table 1. Fibers were collected onto 15 × 15 mm glass coverslips with drop cast PLLA films (50 μL of 4 wt % PLLA/wt $CHCl_3$). The resulting fiber scaffolds were coated with *B. mori* silk fibroin (SF) using the methods described below. Both coated and uncoated scaffolds were sterilized in ethanol (70%) overnight prior to cell culture. Fibers from 3 to 4 independently fabricated batches per group were used for each test ($n$ = 3–4 independently fabricated batches).

### Silk-Coating Procedure.

Nanothin SF coatings were formed on electrospun fiber scaffolds and drop cast films following a previously published coating procedure.[31] Briefly, commercially purchased stock solutions of SF (~100 kDa, extracted and purified from the threads of domesticated *B. mori* silkworm cocoons), was centrifuged at 8400 rcf for 30 min to remove protein aggregates immediately prior to use. SF concentration was then measured using a NanoDrop 1000 Spectrophotometer. The coating solution was prepared by diluting the SF to 0.5 mg/mL using 10 mM Bicine buffer (pH 8.50) and by addition of 200 mM $KH_2PO_4$ added immediately before coating. Electrospun scaffolds were immersed in freshly prepared coating solution in small Petri dishes sealed with parafilm and placed on an incubated orbital shaker (60 rpm) at room temperature (RT). Scaffolds were coated for 12 and 24 h in SF solution, as ellipsometry experiments showed coating thickness is under 20 nm for these incubations; this ensured the surface nanotopography was not completely filled in by the silk coating (Figure S4A). After either 12 or 24 h, scaffolds were removed from the coating solution and vigorously washed with ultrapure water from a squeeze bottle for at least 30 s and dried using a stream of air parallel to fiber alignment to mitigate any rearrangement of the fibers. Care was taken to ensure that the scaffolds did not dry out before the wash step.

### Scanning Electron Microscopy.

In preparation for scanning electron microscopy (SEM), fiber scaffolds with and without SF coatings were sputter coated with approximately 0.75 nm of Au/Pd using a Hummer V Technics sputter coater. An FEI Versa 3D Dual Beam SEM was used to image the surface morphology of fiber scaffolds. Using an accelerating voltage of 2 kV, 4 fields of view near the corners of each coverslip and one near the center were imaged at random for each independently fabricated batch of scaffolds ($n$ = 3 independently fabricated batches) with a working distance of 10 mm and spot size of 5.0. For macroscale analyses, images were taken at 2000× magnification, while for nanoscale assessment, images were taken at 10 000×.

### Fiber Morphology Analysis.

Using images obtained by SEM, fiber morphology was analyzed using the image analysis software FIJI. As cells respond to differences in fiber morphology, fiber diameter, surface coverage, and alignment were measured. A total of 15 pitted, 15 smooth, and 17 divoted images were taken of a combined 3 batches of each fiber type ($n = 3$ independently fabricated batches) at 2000× magnification. The scale was set to 20 $\mu$m, and using the straight-line segment tool, the diameter and alignment of each fiber were measured by zooming in to 150% for accuracy. Only the left side of each image was examined to avoid repeated counting of any fiber. Fiber diameters were measured by drawing a segmented line perpendicular to the fiber, and the average fiber diameter was calculated for each batch. A weighted average was calculated by first taking the product of the percentage of total fibers present in each batch and the average diameter of that batch then summing these products. Diameters of overlapping fibers were not measured. For fiber alignment, fibers were measured by drawing a segmented line parallel to the fiber orientation; the median angle of segmented lines in each image was subtracted from all other segmented line angles in the image. This angle of deviation was then plotted on a histogram as the percentage of fibers with each angle of deviation. Fiber surface coverage was calculated by multiplying the fiber count of the 7207 $\mu m^2$ fields of view by the average fiber diameter for each field of view and dividing by the area (7207 $\mu m^2$) of the image. For each batch of fibers, the average density and standard deviation were calculated and used to obtain the weighted average density and deviation as described above for diameter.

### FTIR Analysis.

FITR analysis was performed with a Bruker Vertex 70 Spectrometer equipped with a Bruker Platinum attenuated total reflection (ATR) diamond crystal cell. Measurements were performed with 100 scans and a resolution of 4 $cm^{-1}$ between wavenumber range of 600–4000 $cm^{-1}$. As PLLA showed absorbance within the amide I area of interest, thus complicating data analysis, $TiO_2$ wafer substrates coated using the same protocol were used instead. Deconvolution of the spectra covering the amide I region (1595–1705 $cm^{-1}$) was performed using Igor Pro. Second derivatives of the spectra were used to calculate peak positions, which were fit with Gaussian distributions. The areas of single bands based on Hu et al.[34] were used to determine the fraction of various secondary structures. Absorption bands within the frequency range of 1616–1637 and 1695–1705 $cm^{-1}$ represented enriched $\beta$-sheet structure while bands in the frequency range of 1638–1655 $cm^{-1}$ were attributed to random coil, 1656–1663 $cm^{-1}$ were attributed to $\alpha$-helices, and 1663–1695 $cm^{-1}$ were attributed to $\beta$-turns.

### Contact Angle.

Surface wettability of electrospun fibers was assessed by measuring static water contact angle using a Kruss DSA100 Drop Shape Analyzer. Fiber scaffolds on coverslips were placed onto the stage between the illuminator and camera with the alignment of the fibers parallel to the orientation of the camera. Three microliters of water were dropped perpendicular to the fiber surface. The angle at the solid–liquid and the liquid–vapor interface was fit using the Drop Shape Analysis 4 software. The left and right side

measurements were averaged for each droplet. A minimum of 3 fiber scaffolds of each type, one from each independently fabricated batch, was analyzed ($n$ = 3 independently fabricated batches).

### ζ-Potential.

ζ-potential experiments could not be conducted with fibers because of instrument limitations. Thus, drop cast PLLA films were used in place of electrospun PLLA fibers for these experiments. PLLA films were drop cast from chloroform (4% w/w: 75 μL onto 18 × 18 mm glass coverslips) and were dried under vacuum overnight. To characterize the surface charge of coated and uncoated PLLA films, ζ-potential measurements were performed using the Anton Paar SurPASS 3 Electrokinetic Analyzer for solid surface analysis, equipped with an integrated titration unit and adjustable gap cell. Experiments were run using a 10 mM KCl electrolyte solution with a pH scan from 2.0 to 10.0 with a pH step of 0.5, and 4 measurements taken at each pH. Three pH scan experiments were done for both 12- and 24-h coated samples, as well as for bare PLLA sample ($n$ = 3 films per condition with 4 measurements taken at each pH).

### FITC Tagging SF-Coated Scaffold.

To visualize the homogeneity of SF coatings on PLLA fibers, fluorescein isothiocyanate (FITC) tagging of SF-coated scaffolds was performed using a protocol adapted from the ThermoFisher FluoReporter FITC Protein Labeling Kit where FITC covalently conjugates to the primary amines of SF. Briefly, scaffolds were coated with SF using the standard silk-coating procedure for either 12 or 24 h, as previously described, and an uncoated scaffold was used as a control. To complete the tagging reaction, FITC (0.2 mg, stock solution of 10 mg/mL FITC in DMSO) was added to sodium bicarbonate buffer (1.5 mL of 100 mM) at pH 9.0. The tagging reaction was covered with aluminum foil and allowed to incubate at RT for 1 h. After 1 h, the scaffolds were removed from the tagging solution and heavily washed (~25 mL) with ultrapure water for 30 s to remove any untagged FITC. The scaffolds were then dried under steady air flow and protected from light until imaging.

### FITC Imaging SF-Coated Scaffold.

Scaffolds were inverted into Pelco imaging dishes on an Olympus IX-81 Confocal Microscope. Using Metamorph Premier 7.7.3.0 imaging software, the scaffolds were imaged at 40× magnification to visualize individual fibers. Images were first taken using brightfield microscopy to ensure that a field of view containing fibers was imaged, and subsequently, the FITC filter was used to image the FITC-tagged SF on the surface of the fibers. A Z-series stack was taken for each field of view of fibers using the same gain (200) and exposure (250 ms) settings to ensure fluorescence signal was FITC-tagged silk and not nonspecific labeling with FITC. Three fields of view on smooth, pitted, and divoted scaffolds that were uncoated, coated with silk for 12 h, or coated with silk for 24 h were imaged to ensure the samples were representative of the entire scaffold ($n$ = 3 technical replicate images for each fiber group).

### Dorsal Root Ganglia Culture.

To determine the effect of surface nanotopography and the SF coatings on neurite outgrowth, dorsal root ganglia (DRG) were cultured on the surface of the fibers. The following procedure was approved by the Rensselaer Polytechnic Institute Institutional Animal Care and Use Committee. P1 Sprague–Dawley rats (Taconic) were euthanized by rapid decapitation. Lumbar and thoracic DRG were extracted and collected in Ham's F-12 Nutrient Mixture on ice. Two DRG were plated in the middle of each fiber scaffold and cultured in neurobasal medium containing B-27 supplement (2% v/v), L-glutamine (0.5 mM), penicillin–streptomycin (1% v/v), and nerve growth factor (50 ng/mL) for 72 h at 37 °C.

### Immunocytochemistry.

Immunocytochemistry was used to assess neurite outgrowth in response to SF-coated fibers. DRG were fixed with paraformaldehyde (4% v/v in phosphate buffered saline; PBS) for 15 min; then, they were washed with PBS twice. DRG were then incubated for 1 h at RT with PBS containing bovine serum albumin (BSA; 5% w/v) and Triton X-100 (0.01% v/v) to prevent nonspecific binding of primary antibody. This was followed by an overnight incubation (>18 h) at 4 °C with primary antibody RT-97 against neurofilament (1:250) in PBS containing BSA (5% w/v) and Tween-20 (1% v/v). DRG were then washed with PBS twice and incubated for 2 h with Alexafluor 488 donkey antimouse secondary antibody (1:1000) at RT. DRG were washed first with 4′,6-diamidino-2-phenylindole (DAPI; 1:1000) in PBS then twice with PBS prior to imaging. Adhesion success of DRG was noted at this point. A minimum of $n = 6$ DRG from 4 separate animals were assessed for DRG adhesion.

### Confocal Microscopy.

DRG on all scaffold types were visualized using an Olympus IX-81 Confocal Microscope and Metamorph Premier 7.7.3.0 imaging software. Imaging for analysis was done at 4× using FITC and 4′,6-diamidino-2-phenylindole (DAPI) filter sets to visualize neurons and nuclei, respectively. A Z-series was taken for each field of view of each DRG with adjustments to gain and exposure to ensure neurites were visible in low signal areas. Consecutive fields of view were imaged to include the entire DRG and neurites. A minimum of $n = 6$ DRG from 4 separate animals were imaged for each fiber group.

### Image Analysis.

ImageJ software was used to stack confocal images of the DRG and subtract background noise (rolling ball radius = 40 pixels). Adobe Photoshop CS2 was then used to stitch successive images together. Composite images were analyzed with ImageJ to measure neurite outgrowth; the five longest neurites on each side of the DRG body were measured and averaged. For this analysis, the average of each side of the DRG was considered a technical replicate. DRG aspect ratio was determined by dividing the longest DRG length (from the end to end of neurites) by the widest width of the DRG. A minimum of $n = 6$ DRG from 4 separate animals were imaged for each fiber group.

### Statistical Analysis.

Statistical analysis was conducted using Minitab 17. Data normality was first assessed using a Ryan–Joiner Test then data were assessed for equal variance. Fiber morphology data were analyzed using Welch's ANOVA with post hoc Games–Howell test. Because of a non-normal distribution, diameter data were represented as a plot of boxplots. Fiber surface coverage data were represented as means ± standard deviation. Alignment data were represented as histograms of the percentage of fibers with a given angle of deviation from the median angle. Fiber contact angle data were represented as means ± standard deviation. Fiber contact angle differences were assessed using Welch's ANOVA with post hoc Games–Howell test. $\zeta$-Potential data were plotted as a scatter plot of the means ± standard deviation of 4 technical replicate measurements at each pH value. The isoelectric point (pI) was calculated for 3 separate batches of each coating type. Isoelectric points were compared via a one-way ANOVA with post hoc Dunnett's test. To assess whether DRG adhered better to different scaffold types, binary logistic regression was used, with and without adjustment. Finally, Welch's ANOVA with post hoc Games–Howell test was used to assess differences in neurite outgrowth and aspect ratio between fiber groups. More detailed statistical information is included in Tables S3–S21.

## RESULTS AND DISCUSSION

In this study, we aimed to enhance DRG adhesion and neurite outgrowth on PLLA fibers with varying surface nanotopography using thin films of SF. First, SEM was used to assess differences in fiber physical characteristics (Figure 1A–1C). Fiber diameter ($F[2] = 11.61$, $p < 0.001$; Figure 1D) and fiber surface coverage on PLLA films ($F[2] = 4.29$, $p = 0.024$; Figure 1E) were greater for fibers with divoted surfaces compared to smooth and pitted fibers. Fiber alignment was similar between groups regardless of surface nanotopography ($F[2] = 2.14$, $p = 0.118$; Figure 1F).

It was previously demonstrated that electrospun fiber diameter is directly correlated to changes in humidity, where increased humidity resulted in greater diameter of polystyrene fibers.[35] Thus, the increased humidity required to produce surface divots (Table 1) likely contributes to the slight increase in fiber diameter observed here. Wang et al. demonstrate that increased fiber diameter, above 750 nm, results in more neurite outgrowth compared to DRG on lower nanodiameter fibers.[5] In addition to greater diameter, a greater surface coverage by divoted fibers compared to smooth and pitted was observed. Thus, the combination of slightly larger diameter and more surface to anchor to on divoted fibers may enhance adhesion of DRG and/or the density of neurites that extend from the DRG body.

To macroscopically visualize SF coatings on PLLA fibers, Congo Red was used to stain for $\beta$-sheet structures found in SF (please see Figure S1). Both 12- and 24-h coated scaffolds showed a homogeneous red tint after staining, independent of surface nanotopography, while uncoated scaffolds exhibited no red hue (Figure S1). The molecular conformations of the nanothin silk coatings were further investigated using FTIR to verify the results of Congo Red staining. Notably, absorption bands between 1616–1637 and 1695–1705 $cm^{-1}$ were observed, suggesting that coatings were enriched in $\beta$-sheet structures.[34] A high degree of $\beta$-sheets (28.5% and 38.6%) was found for both untreated and ethanol treated 24 h coatings,

respectively (Figure S2). These results correlate well with secondary structures previously found in silk fibroin particles fabricated by salting out with potassium phosphate,[36] as well as that of ethanol treated ultrathin recombinant spider silk films of approximately the same thickness.[37]

Coating uniformity on a microscopic scale was further investigated using fluorescence confocal microscopy. As neither SF nor PLLA innately fluoresce, SF coatings were labeled with fluorescein isothiocyanate (FITC), a commonly used fluorophore that efficiently conjugates to the primary amines of proteins. Figure 2 shows fluorescent and brightfield images of uncoated, 12-h silk coated, and 24-h silk coated divoted fiber scaffolds. The brightfield images confirmed that fibers were present in each imaged field of view (Figure 2 bottom row), while the fluorescent images demonstrated that the SF coatings cover the entirety of each fiber, as well as fibers of various scaffold depths (Figure 2 top row). This was seen for all coated scaffolds independent of surface nanotopography (Figure S3). Furthermore, it was confirmed that uncoated PLLA fibers showed no fluorescence intensity with the same exposure settings because of the inability of the FITC to react with PLLA. This result clearly demonstrates the difference in the surface chemistry between coated and uncoated fibers. Importantly, from the brightfield images, the SF coatings do not appear to significantly alter PLLA fiber diameter nor orientation following the coating process, suggesting nano-thickness.

Since FITC-labeling demonstrated the homogeneous coverage of PLLA fibers with SF, we assessed the static water contact angle of coated and uncoated scaffolds to determine changes in hydrophobicity (Figure 3A). Though bulk SF is slightly more hydrophilic than PLLA, no significant differences in surface wettability were observed between uncoated and silk coated fibers of respective nanotopographies (Tables S6–S8) likely because of the high surface roughness of the scaffolds. There is a slight, though insignificant, trend of decreased water contact angle with increased duration of SF coating time (Figure 3B).

The propensity of cells to adhere to silk surfaces is well-documented, and aside from surface wettability and topography, surface charge is another important factors influencing cell adhesion.[38] Therefore, the $\zeta$-potentials of bare PLLA and SF-coated PLLA in a 10 mM KCl electrolyte solution were investigated using a SurPASS 3 electrokinetic analyzer instrument (Figure 4). Coated and uncoated PLLA appear to have similar $\zeta$-potentials above pH 6, suggesting similar surface charge densities above a pH of 6.0. However, a clear shift in the isoelectric point (pI) from approximately 3–4 for uncoated and SF-coated PLLA, respectively, is observed. This change in pI signifies a change in surface chemistry to more basic functional groups likely due to the presence of lysine, arginine, and histidine found in the primary structure of both the light and heavy chain of SF[39,40] (Table 2; $F[8] = 43.61$, $p < 0.001$). This increase in the pI corresponds well with literature values of pI = 4.39 for the SF heavy chain,[38] especially since the SF used in our studies is a hydrolyzed fragment (~100 kDa) of the native protein (~350 kDa), which could account for the small discrepancy. Although it is difficult to directly correlate $\zeta$-potential with cell adhesion, the change in surface chemistry, as verified by FITC-labeling and isoelectric point shift, may be beneficial for promoting cell adhesion and neurite outgrowth by providing a less negatively charged

surface (pI = 4 vs pI = 3). Surfaces with highly negative charges have been known to interfere with cell–matrix interactions, therefore hindering cell spreading.[38]

On the basis of changes in surface chemistry of the scaffolds, we attempted to quantify the thickness of SF by ellipsometry, a common spectroscopic technique used to measure thin film thickness on planar substrates. However, ellipsometry is unsuitable for fiber scaffolds and, moreover, could not be performed on SF-coated drop cast PLLA films due to lifting of the films from the supporting glass coverslip. Thus, to estimate the thickness of SF coatings, the identical coating process was used to generate SF coatings on atomically flat $TiO_2$-coated Si wafers (please see Supporting Information). Ellipsometry performed on these wafers suggested that SF coating thickness ranges from 12–16 nm for 12–24 h coatings (Figure S4A). SEM of pitted fibers with 12-h SF coatings supported this result, as some surface pitting remained visible after coating. Since pits range from 50 to 200 nm[8] in size, it is reasonable to estimate the SF coating on PLLA fibers to be tens of nanometers thick at most. Additionally, thin ribbons of SF spanning the gap between fibers was sometimes observed (Figure S4C).

There are many methods reported in literature for fabricating SF coatings and films, such as drop casting, spin coating, and dip coating.[41] Using these methods, coating thickness can be tuned through parameters, such as SF concentration, dip coating rate, and casting volume. However, dip coating and drop casting methods generally produce coatings that are tens to hundreds of microns thick,[42,43] while spin coating is only applicable for planar substrates with minimal surface roughness.[44] Layer-by-layer deposition has been explored as a method to produce nanothin SF coatings but requires tedious processing and organic solvents to produce insoluble films.[45] Thus, to our knowledge, our work is the first example of the formation of nanothin SF coatings on nonplanar substrates with complex nanotopographies.

After confirming (1) a change in fiber surface chemistry and (2) persistence of surface nanotopography post coating, we assessed the neuroregenerative capabilities of the scaffolds by assessing DRG adhesion and neurite extension on fibers with SF coatings. Hu et. al previously found that Schwann cells adhered well to electrospun SF nanofibers, promoting cell viability and proliferation,[19] which is critical in the application of the silk-based materials for nerve regeneration. In our study, DRG containing neurons and Schwann cells were plated on smooth, pitted, and divoted fibers with no coating, a 12-h SF coating, or a 24-h SF coating to determine the percent adhesion of the DRG bodies. An increasing trend in DRG adhesion with increased duration of SF coating was observed (Figure 5), particularly for smooth and divoted fibers ($\chi^2[2] = 11.28$, $p = 0.004$). Although not statistically different, adhesion on uncoated pitted fibers was approximately 20% greater compared to uncoated smooth and divoted fibers (Figure 5). This is consistent with a study by Fozdar et al., which demonstrated that rat hippocampal neurons preferentially extend on nanomicroporous quartz surfaces over smooth quartz surfaces.[7]

In addition to examining the impact of SF coatings on DRG adhesion, we also assessed effects on neurite outgrowth, which is most indicative of regenerative efficacy of the scaffolds. DRG were labeled using immunocytochemistry for neurofilament and imaged on all fiber types using confocal microscopy (please see Figure S5; sample images for DRG on

the divoted fiber groups are shown in Figure 6A–C). For uncoated fibers, neurite outgrowth was typically shorter on pitted and divoted fibers compared to smooth fibers (Figure 6D), though this trend was not statistically significant. Neurite outgrowth was significantly improved on silk-coated pitted and divoted fibers compared to uncoated pitted and divoted fibers, respectively (Figure 6D; $F[8] = 15.73$, $p < 0.001$). Similarly, DRG aspect ratio was significantly greater on 12- and 24-h silk-coated pitted fibers and 12-h silk-coated divoted fibers compared to the uncoated controls (Figure 6E; $F[8] = 6.50$, $p < 0.001$). Improvement in aspect ratio and neurite extension was also observed for smooth fibers, though this result was not statistically significant.

Our results of DRG adhesion and neurite outgrowth on uncoated fibers are surprising. As discussed previously, studies have shown that neurites better extend on surfaces with 300 nm–2 $\mu$m topologies compared to smooth surfaces,[7] which is partially confirmed by our results showing trends of increased adhesion on uncoated pitted fiber surfaces compared to smooth and divoted surfaces. However, outgrowth on uncoated pitted and divoted fibers was typically lower compared to smooth fibers. It is possible that the regenerative efficacy is extremely dependent on topography size, and the topography on our pitted and divoted fibers are too small (~50–200 nm) to promote neurite outgrowth. This suggests that topographical cues in the high nanometer/low micron range are likely to have the most beneficial effect. However, the effect of the SF coating on improving DRG adhesion and neurite outgrowth is quite robust. The silk coating not only outweighs the effect of topography but further enhances outgrowth compared to uncoated controls. Ultimately, our results suggest that having topography is somewhat important for cell adhesion but having a bioactive surface coating is most important for the promotion of neurite outgrowth.

As more significant changes in neurite outgrowth were observed with coated pitted and divoted fibers, this suggests that surface nanotopography may have influenced the adsorption of SF to the fiber surface. The influence of nanotopography on protein adsorption has been extensively studied and has been shown to affect protein binding,[46] as well as subsequent cell binding[46,47] in several ways. For example, surface nanotopography may alter the geometrical packing of proteins or act as preferred adsorption sites for the protein, creating patterns similar to the underlying nanotopography. Proteins with conformations much smaller or larger than the scale of the nanotopography may change in conformation upon adsorption,[46] affecting the exposure of certain functional groups cell-surface interactions. Furthermore, the diameter of divoted fibers, which showed the greatest neurite outgrowth and aspect ratio after coating with SF, was slightly larger than smooth and pitted fibers (Figure 1); the difference in fiber curvature based on fiber diameter may also play a role in silk adsorption. Roach et al. found that when the globular protein BSA was bound to particles with high surface curvature, BSA's structure was stabilized. Conversely, when the rod-like protein fibrinogen was bound to the same surface, the acute change in the surface angle caused the fibrinogen to wrap around the particle and lose some of its secondary structure.[48] Thus, the microscale topography of the fibers themselves and the nanoscale topologies present on the surface may both influence protein adsorption and cell adhesion.

In a previous study by our group, D'Amato et al. cultured DRG on laminin coated smooth, pitted, and divoted fibers and found that the laminin coating, which is commonly used as a

substrate for neurons in vitro, approximately doubled the neurite extension of DRG on all fiber topographies. D'Amato et al. also demonstrated that laminin masked differences in outgrowth from topography on uncoated substrates.[10] Similarly, we observed that DRG neurite outgrowth was approximately doubled after 3 days on silk coated fibers and that while uncoated fibers had a trend of reduced outgrowth with the presence of surface nanotopography, our nanothin SF coatings appeared to mask this effect. Taken together, these results surprisingly suggest that SF can potentially promote neurite outgrowth similar to laminin, a protein known for its ability to promote neuron adhesion and neurite outgrowth. However, a comprehensive comparison of the effects of SF and laminin on neural cells has not been reported and is outside the scope of this work. While laminin has a C-terminal integrin binding domain that promotes cell adhesion,[49] the mechanism of the benefit of SF on neural cell adhesion is largely unknown. Many studies characterizing silk biomaterials have attempted to improve cell affinity for silk by incorporating binding motifs. Studies have synthesized recombinant spider silk proteins with various cell binding motifs, including RGD and IKVAV,[50] as well as coupled RGD to SF[51] to enhance biocompatibility. In our work, we demonstrated that added binding domains were not necessary to promote DRG adhesion and neurite outgrowth. Other studies have compared the responses of nervous system cells on silk surfaces to poly-L-lysine coated surfaces because poly-L-lysine is also commonly used to promote attachment of neural cells for cell culture. These studies demonstrated that SF nanofibers promote Schwann cell adhesion and proliferation,[19] as well as neurite outgrowth and astrocyte spreading[21] similar to poly-L-lysine-coated surfaces, further supporting the benefit of SF coatings for neural cell integration with biomaterials. Additional binding domains may further enhance adhesion and outgrowth on silk-coated surfaces, and the cellular mechanism of improved DRG adhesion and neurite extension on nanothin silk coatings should be studied further.

## CONCLUSIONS

In this study, we demonstrated the ability to form nanothin SF coatings by controlled self-assembly onto electrospun PLLA fibers with various complex nanotopographies. These SF coatings coat fibers homogeneously, altering their surface chemistry without significantly changing the surface nanotopography. To our knowledge, our work is the first example of noncovalent SF coating formation on topographically complex surfaces, as conventional dip coating, spin coating, and drop-casting coating methods are poorly suited for nonplanar substrates with fine features. We observed greater DRG adhesion and neurite outgrowth on fibers with SF coatings, particularly when the fibers had pitted or divoted surfaces. Furthermore, SF coatings may be a promising option to enhance polymer scaffold biocompatibility for other nervous system cells. In a pilot study, we demonstrated that spinal cord astrocytes cover a much greater area of the fiber scaffolds when coated with nanothin SF for 12 h; this enhancement in astrocyte surface coverage is most pronounced when divoted fibers are coated with silk fibroin (Figure S6).

As SF coating formation is an aqueous, noncovalent process that does not utilize chemical cross-linking, the facile incorporation of bioactive molecules that enhance neuroregenerative efficacy, such as nerve growth factor and other neurotrophins, by "co-coating" with SF may be explored in future studies. Incorporation of these proteins in their active conformation is

currently challenging during electrospun scaffold fabrication, as the electrospinning process often uses organic solvents that denature biological components. Moreover, studies have demonstrated stabilization and delivery of interferon-$\gamma$ and interleukin-4 in various silk-based hydrogels[52] and films,[53] while glucose oxidase, lipase, and horseradish peroxidase encapsulated in SF films exhibit some bioactivity after a minimum of 5 months storage.[54] Thus, our new strategy of coating topographically complex surfaces with SF, which enhances cell adhesion and neurite outgrowth, serves as a versatile platform for future exploration of multifunctional silk-modified electrospun scaffolds for neural regeneration.

## Supplementary Material

Refer to Web version on PubMed Central for supplementary material.

## ACKNOWLEDGMENTS

We thank Troy Vargason for teaching binary logistic regression analysis, Neda Bajalo and the Bioresearch Core for their assistance with animal care, Joel Morgan and the Analytical Biochemistry Core for their assistance with FTIR, and Deniz Rende and the Nanoscale Characterization Core for their assistance with electron microscopy.

Funding

This work received partial support from R01 (NINDS) NS092754 to R.J.G. and NY State Spinal Cord Injury Grant C32245GG to R.J.G. This manuscript is based upon work supported by the National Science Foundation Graduate Research Fellowship Program under Grant DGE-1247271 to A.M.Z.

## ABBREVIATIONS

| | |
|---|---|
| **BSA** | bovine serum albumin |
| **$CHCl_3$** | chloroform |
| **DMSO** | dimethyl sulfoxide |
| **DRG** | dorsal root ganglia |
| **FITC** | fluorescein isothiocyanate |
| **pI** | isoelectric point |
| **PBS** | phosphate buffered saline |
| **PLLA** | poly-L-lactic acid |
| **RT** | room temperature |
| **SEM** | scanning electron microscopy |
| **SF** | silk fibroin |

## REFERENCES

(1). Frost HK; Andersson T; Johansson S; Englund-Johansson U; Ekström P; Dahlin LB; Johansson F Electrospun Nerve Guide Conduits Have the Potential to Bridge Peripheral Nerve Injuries in Vivo. Sci. Rep 2018, 8 (1), 16716. [PubMed: 30425260]

(2). Wang Y; Kong Y; Zhao Y; Feng Q; Wu Y; Tang X; Gu X; Yang Y Electrospun, Reinforcing Network-Containing, Silk Fibroin-Based Nerve Guidance Conduits for Peripheral Nerve Repair. Journal of Biomaterials and Tissue Engineering 2019, 6 (1), 53–60.

(3). Hurtado A; Cregg JM; Wang HB; Wendell DF; Oudega M; Gilbert RJ; McDonald JW Robust CNS Regeneration after Complete Spinal Cord Transection Using Aligned Poly-L-Lactic Acid Microfibers. Biomaterials 2011, 32 (26), 6068–6079. [PubMed: 21636129]

(4). Gelain F; Panseri S; Antonini S; Cunha C; Donega M; Lowery J; Taraballi F; Cerri G; Montagna M; Baldissera F; Vescovi A Transplantation of Nanostructured Composite Scaffolds Results in the Regeneration of Chronically Injured Spinal Cords. ACS Nano 2011, 5 (1), 227–236. [PubMed: 21189038]

(5). Wang HB; Mullins ME; Cregg JM; McCarthy CW; Gilbert RJ Varying the Diameter of Aligned Electrospun Fibers Alters Neurite Outgrowth and Schwann Cell Migration. Acta Biomater. 2010, 6 (8), 2970–2978. [PubMed: 20167292]

(6). Yoon S-D; Kwon Y-S; Lee K-S Biodegradation and Biocompatibility of Poly L-Lactic Acid Implantable Mesh. Int. Neurourol. J 2017, 21 (Suppl1), S48–54. [PubMed: 28446016]

(7). Fozdar DY; Lee JY; Schmidt CE; Chen S Selective Axonal Growth of Embryonic Hippocampal Neurons According to Topographic Features of Various Sizes and Shapes. Int. J. Nanomed 2010, 6, 45–57.

(8). Schaub NJ; Britton T; Rajachar R; Gilbert RJ Engineered Nanotopography on Electrospun PLLA Microfibers Modifies RAW 264.7 Cell Response. ACS Appl. Mater. Interfaces 2013, 5 (20), 10173–10184.

(9). Schaub NJ; D'Amato AR; Mason A; Corr DT; Harmon EY; Lennartz MR; Gilbert RJ The Effect of Engineered Nanotopography of Electrospun Microfibers on Fiber Rigidity and Macrophage Cytokine Production. J. Biomater. Sci., Polym. Ed 2017, 28, 1303–1323. [PubMed: 28420296]

(10). D'Amato AR; Puhl DL; Ziemba AM; Johnson CDL; Doedee J; Bao J; Gilbert RJ Exploring the Effects of Electrospun Fiber Surface Nanotopography on Neurite Outgrowth and Branching in Neuron Cultures. PLoS One 2019, 14 (2), e0211731. [PubMed: 30716106]

(11). Johnson CD; D'Amato AR; Puhl DL; Wich DM; Vesperman A; Gilbert RJ Electrospun Fiber Surface Nanotopography Influences Astrocyte-Mediated Neurite Outgrowth. Biomed. Mater 2018, 13 (5), 054101. [PubMed: 29762127]

(12). Ziemba AM; Lane KP; Balouch B; D'Amato AR; Totsingan F; Gross RA; Gilbert RJ Lactonic Sophorolipid Increases Surface Wettability of Poly-L-Lactic Acid Electrospun Fibers. ACS Appl. Bio Mater 2019, 2, 3153.

(13). Meinel L; Hofmann S; Karageorgiou V; Kirker-Head C; McCool J; Gronowicz G; Zichner L; Langer R; Vunjak-Novakovic G; Kaplan DL The Inflammatory Responses to Silk Films in Vitro and in Vivo. Biomaterials 2005, 26 (2), 147–155. [PubMed: 15207461]

(14). Lu Q; Hu X; Wang X; Kluge JA; Lu S; Cebe P; Kaplan DL Water-Insoluble Silk Films with Silk I Structure. Acta Biomater. 2010, 6 (4), 1380–1387. [PubMed: 19874919]

(15). Lu Q; Zhang B; Li M; Zuo B; Kaplan DL; Huang Y; Zhu H Degradation Mechanism and Control of Silk Fibroin. Biomacromolecules 2011, 12 (4), 1080–1086. [PubMed: 21361368]

(16). Vepari C; Kaplan DL Silk as a Biomaterial. Prog. Polym. Sci 2007, 32 (8–9), 991–1007. [PubMed: 19543442]

(17). Thurber AE; Omenetto FG; Kaplan DL In Vivo Bioresponses to Silk Proteins. Biomaterials 2015, 71, 145–157. [PubMed: 26322725]

(18). Yang Y; Chen X; Ding F; Zhang P; Liu J; Gu X Biocompatibility Evaluation of Silk Fibroin with Peripheral Nerve Tissues and Cells in Vitro. Biomaterials 2007, 28 (9), 1643–1652. [PubMed: 17188747]

(19). Hu A; Zuo B; Zhang F; Lan Q; Zhang H Electrospun Silk Fibroin Nanofibers Promote Schwann Cell Adhesion, Growth and Proliferation. Neural Regen Res. 2012, 7 (15), 1171–1178. [PubMed: 25722711]

(20). Tang X; Ding F; Yang Y; Hu N; Wu H; Gu X Evaluation on in Vitro Biocompatibility of Silk Fibroin-Based Biomaterials with Primarily Cultured Hippocampal Neurons. J. Biomed. Mater. Res., Part A 2009, 91A (1), 166–174.

(21). Qu J; Wang D; Wang H; Dong Y; Zhang F; Zuo B; Zhang H Electrospun Silk Fibroin Nanofibers in Different Diameters Support Neurite Outgrowth and Promote Astrocyte Migration. J. Biomed. Mater. Res., Part A 2013, 101A (9), 2667–2678.

(22). Wang J; Ye R; Wei Y; Wang H; Xu X; Zhang F; Qu J; Zuo B; Zhang H The Effects of Electrospun TSF Nanofiber Diameter and Alignment on Neuronal Differentiation of Human Embryonic Stem Cells - Wang - 2012 - Journal of Biomedical Materials Research Part A - Wiley Online Library. J. Biomed. Mater. Res., Part A 2012, 100A (3), 632–645.

(23). Tian LP; Prabhakaran M; Hu J; Chen M; Besenbacher F; Ramakrishna S Coaxial Electrospun Poly(Lactic Acid)/Silk Fibroin Nanofibers Incorporated with Nerve Growth Factor Support the Differentiation of Neuronal Stem Cells. RSC Adv. 2015, 5 (62), 49838–49848.

(24). Tsukawaki S; Murakami T; Suzuki K; Nakazawa Y Studies on the Potential Risk of Amyloidosis from Exposure to Silk Fibroin. Biomed. Mater 2016, 11 (6), 065010. [PubMed: 27869107]

(25). Wang H; Shao H; Hu X Structure of Silk Fibroin Fibers Made by an Electrospinning Process from a Silk Fibroin Aqueous Solution. J. Appl. Polym. Sci 2006, 101 (2), 961–968.

(26). Zhu J; Shao H; Hu X Morphology and Structure of Electrospun Mats from Regenerated Silk Fibroin Aqueous Solutions with Adjusting PH. Int. J. Biol. Macromol 2007, 41 (4), 469–474. [PubMed: 17689606]

(27). Yi B; Zhang H; Yu Z; Yuan H; Wang X; Zhang Y Fabrication of High Performance Silk Fibroin Fibers via Stable Jet Electrospinning for Potential Use in Anisotropic Tissue Regeneration. J. Mater. Chem. B 2018, 6 (23), 3934–3945. [PubMed: 32254322]

(28). Li G; Chen K; You D; Xia M; Li W; Fan S; Chai R; Zhang Y; Li H; Sun S Laminin-Coated Electrospun Regenerated Silk Fibroin Mats Promote Neural Progenitor Cell Proliferation, Differentiation, and Survival in Vitro. Front. Bioeng. Biotechnol 2019, DOI: 10.3389/fbioe.2019.00190.

(29). Liu Q; Huang J; Shao H; Song L; Zhang Y Dual-Factor Loaded Functional Silk Fibroin Scaffolds for Peripheral Nerve Regeneration with the Aid of Neovascularization. RSC Adv. 2016, 6 (9), 7683–7691.

(30). Zhang X; Reagan MR; Kaplan DL Electrospun Silk Biomaterial Scaffolds for Regenerative Medicine. Adv. Drug Delivery Rev 2009, 61 (12), 988–1006.

(31). Zha RH; Delparastan P; Fink TD; Bauer J; Scheibel T; Messersmith PB Universal Nanothin Silk Coatings via Controlled Spidroin Self-Assembly. Biomater. Sci 2019, 7 (2), 683–695. [PubMed: 30628598]

(32). Leal-Egaña A; Lang G; Mauerer C; Wickinghoff J; Weber M; Geimer S; Scheibel T Interactions of Fibroblasts with Different Morphologies Made of an Engineered Spider Silk Protein. Adv. Eng. Mater 2012, 14 (3), B67–B75.

(33). Wang HB; Mullins ME; Cregg JM; Hurtado A; Oudega M; Trombley MT; Gilbert RJ Creation of Highly Aligned Electrospun Poly-L-Lactic Acid Fibers for Nerve Regeneration Applications. J. Neural Eng 2009, 6 (1), 016001. [PubMed: 19104139]

(34). Hu X; Kaplan D; Cebe P Determining Beta-Sheet Crystallinity in Fibrous Proteins by Thermal Analysis and Infrared Spectroscopy. Macromolecules 2006, 39 (18), 6161–6170.

(35). Fashandi H; Karimi M Pore Formation in Polystyrene Fiber by Superimposing Temperature and Relative Humidity of Electrospinning Atmosphere. Polymer 2012, 53 (25), 5832–5849.

(36). Lammel AS; Hu X; Park S-H; Kaplan DL; Scheibel TR Controlling Silk Fibroin Particle Features for Drug Delivery. Biomaterials 2010, 31 (16), 4583–4591. [PubMed: 20219241]

(37). Borkner CB; Lentz S; Müller M; Fery A; Scheibel T Ultrathin Spider Silk Films: Insights into Spider Silk Assembly on Surfaces. ACS Appl. Polym. Mater 2019, 1 (12), 3366–3374.

(38). Leal-Egaña A; Scheibel T Interactions of Cells with Silk Surfaces. J. Mater. Chem 2012, 22 (29), 14330–14336.

(39). FIBH—Fibroin heavy chain precursor—Bombyx mori (Silk moth)—FIBH gene & protein. https://www.uniprot.org/uniprot/P05790 (accessed Aug 31, 2019-08-31).

(40). FIBL—Fibroin light chain precursor—Bombyx mori (Silk moth)—FIBL gene & protein. https://www.uniprot.org/uniprot/P21828 (accessed 2019-08-31).

(41). Borkner CB; Elsner MB; Scheibel T Coatings and Films Made of Silk Proteins. ACS Appl. Mater. Interfaces 2014, 6 (18), 15611–15625. [PubMed: 25004395]

(42). Zeplin PH; Maksimovikj NC; Jordan MC; Nickel J; Lang G; Leimer AH; Römer L; Scheibel T Spider Silk Coatings as a Bioshield to Reduce Periprosthetic Fibrous Capsule Formation. Adv. Funct. Mater 2014, 24 (18), 2658–2666.

(43). Agostini E; Winter G; Engert J Water-Based Preparation of Spider Silk Films as Drug Delivery Matrices. J. Controlled Release 2015, 213, 134–141.

(44). Jiang C; Wang X; Gunawidjaja R; Lin Y-H; Gupta MK; Kaplan DL; Naik RR; Tsukruk VV Mechanical Properties of Robust Ultrathin Silk Fibroin Films. Adv. Funct. Mater 2007, 17 (13), 2229–2237.

(45). Wang X; Kim HJ; Xu P; Matsumoto A; Kaplan DL Biomaterial Coatings by Stepwise Deposition of Silk Fibroin. Langmuir 2005, 21 (24), 11335–11341. [PubMed: 16285808]

(46). Lord MS; Foss M; Besenbacher F Influence of Nanoscale Surface Topography on Protein Adsorption and Cellular Response. Nano Today 2010, 5 (1), 66–78.

(47). Sutherland DS; Broberg M; Nygren H; Kasemo B Influence of Nanoscale Surface Topography and Chemistry on the Functional Behaviour of an Adsorbed Model Macromolecule. Macromol. Biosci 2001, 1 (6), 270–273.

(48). Roach P; Farrar D; Perry CC Surface Tailoring for Controlled Protein Adsorption: Effect of Topography at the Nanometer Scale and Chemistry. J. Am. Chem. Soc 2006, 128 (12), 3939–3945. [PubMed: 16551101]

(49). Aumailley M The Laminin Family. Cell Adhes. Migr 2013, 7 (1), 48–55.

(50). Widhe M; Johansson U; Hillerdahl C-O; Hedhammar M Recombinant Spider Silk with Cell Binding Motifs for Specific Adherence of Cells. Biomaterials 2013, 34 (33), 8223–8234. [PubMed: 23916396]

(51). Chen J; Altman GH; Karageorgiou V; Horan R; Collette A; Volloch V; Colabro T; Kaplan DL Human Bone Marrow Stromal Cell and Ligament Fibroblast Responses on RGD-Modified Silk Fibers. J. Biomed. Mater. Res 2003, 67 (2), 559–570.

(52). Kumar M; Coburn J; Kaplan DL; Mandal BB Immuno-Informed 3D Silk Biomaterials for Tailoring Biological Responses. ACS Appl. Mater. Interfaces 2016, 8 (43), 29310–29322. [PubMed: 27726371]

(53). Reeves ARD; Spiller KL; Freytes DO; Vunjak-Novakovic G; Kaplan DL Controlled Release of Cytokines Using Silk-Biomaterials for Macrophage Polarization. Biomaterials 2015, 73, 272–283. [PubMed: 26421484]

(54). Lu S; Wang X; Lu Q; Hu X; Uppal N; Omenetto FG; Kaplan DL Stabilization of Enzymes in Silk Films. Biomacromolecules 2009, 10 (5), 1032–1042. [PubMed: 19323497]

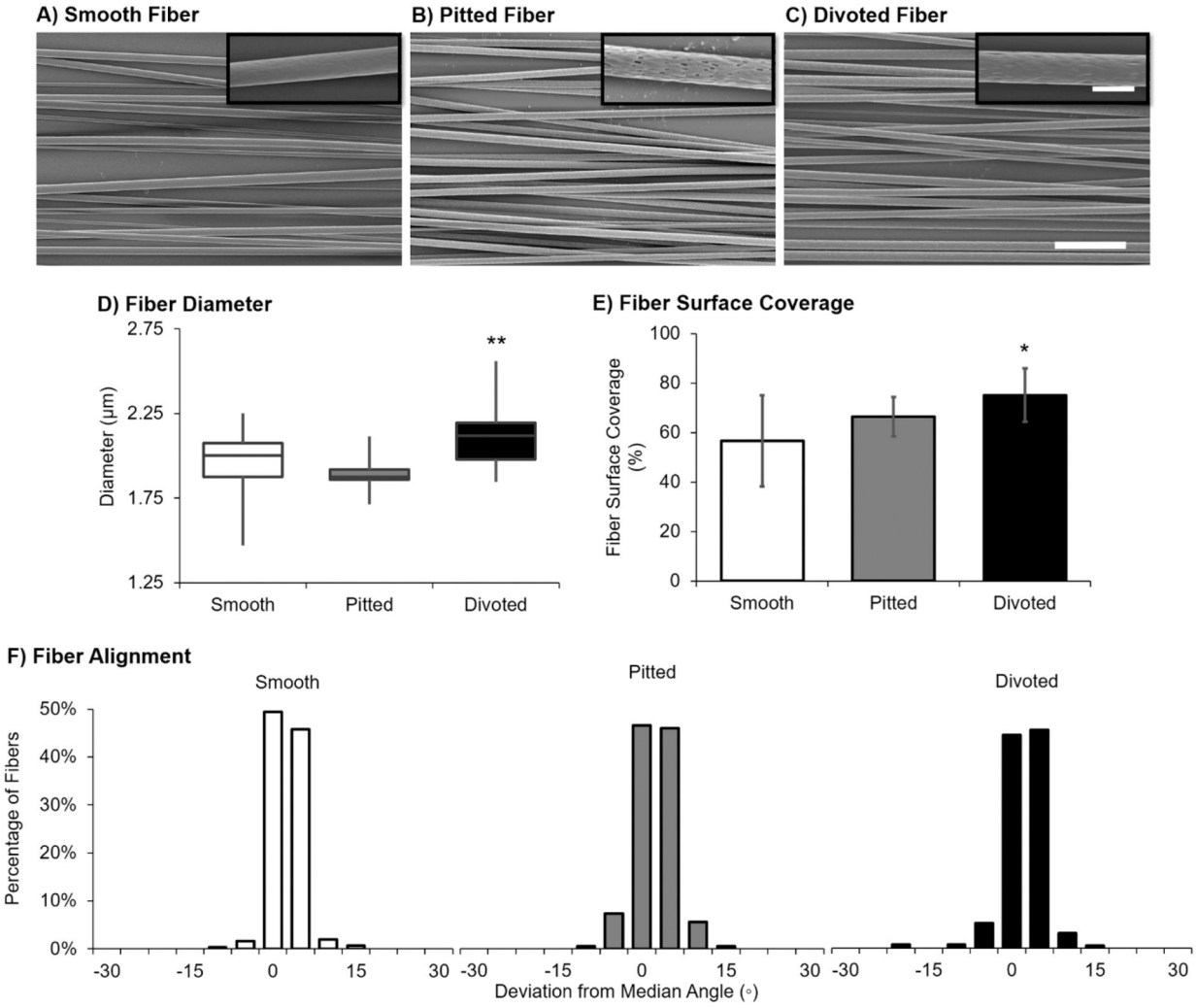


**Figure 1.**

Uncoated fibers with varying surface nanotopographies have similar microscale surface characteristics. SEM image of (A) smooth, (B) pitted, and (C) divoted fibers, scale bar for 2000× magnification images = 20 $\mu$m and scale bar for 15000× magnification images = 3 $\mu$m. (D) Fiber diameter data (in $\mu$m) are represented as a plot of boxplots. (E) Fiber surface coverage is represented as the mean percentage of surface covered by fibers ± standard deviation. (F) Fiber alignment is represented as a set of histograms of the percentage of each type of fibers with a deviation from the median fiber angle in degrees. Statistical differences compared to the smooth fiber control were assessed using Welch's ANOVA with post hoc Games–Howell test (*$p < 0.05$; **$p < 0.001$). For all assessments, a minimum of 15 fields of view from $n = 3$ independently fabricated batches were characterized.

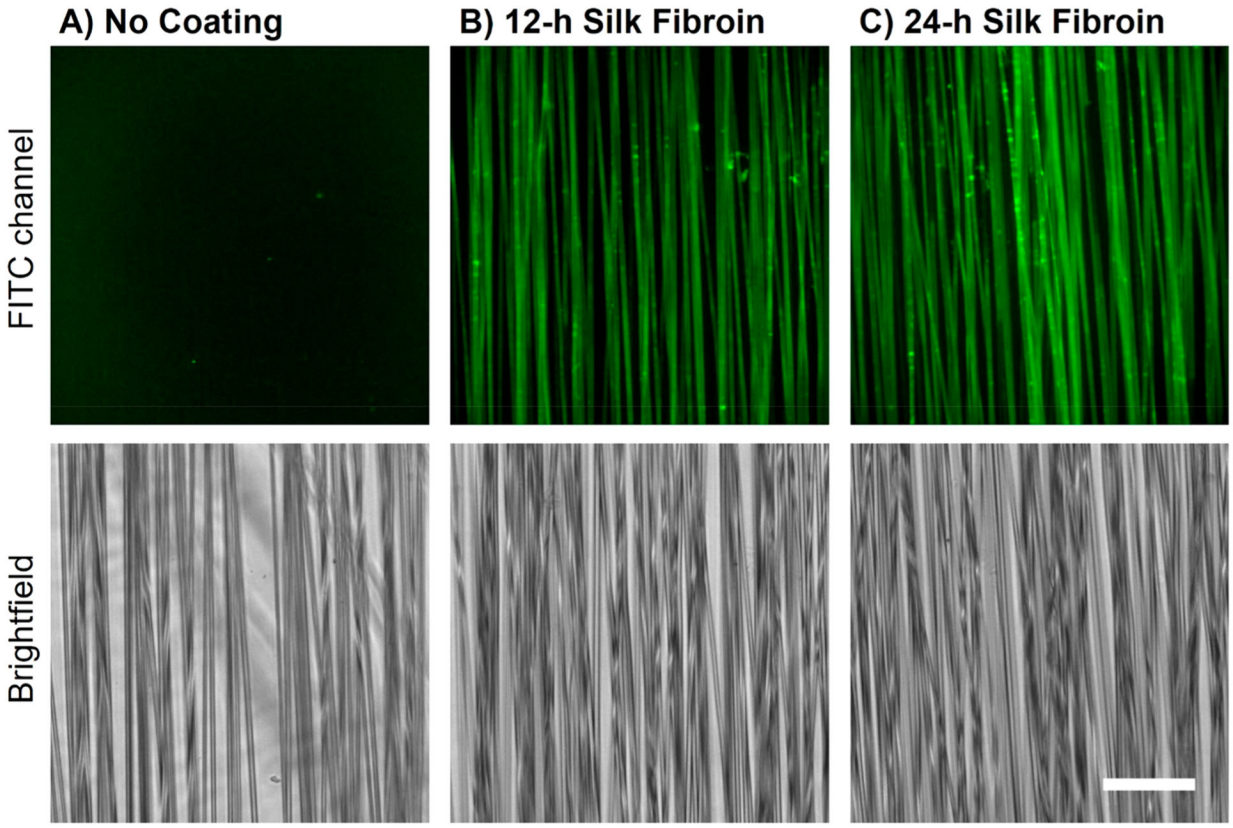


**Figure 2.**

SF-coated divoted fibers can be labeled with FITC while fibers without SF exhibit no fluorescence. Sample images of divoted fibers that have (A) no coating, (B) 12-h SF coating, or (C) 24-h SF coating (scale bar = 50 $\mu$m). The top row displays the FITC channel fluorescence images, while the bottom row displays the brightfield images of the same field of view. Three fields of view were imaged on each scaffold to ensure the sample images were representative of the entire scaffold. (Other fiber types are displayed in Supporting Information.)

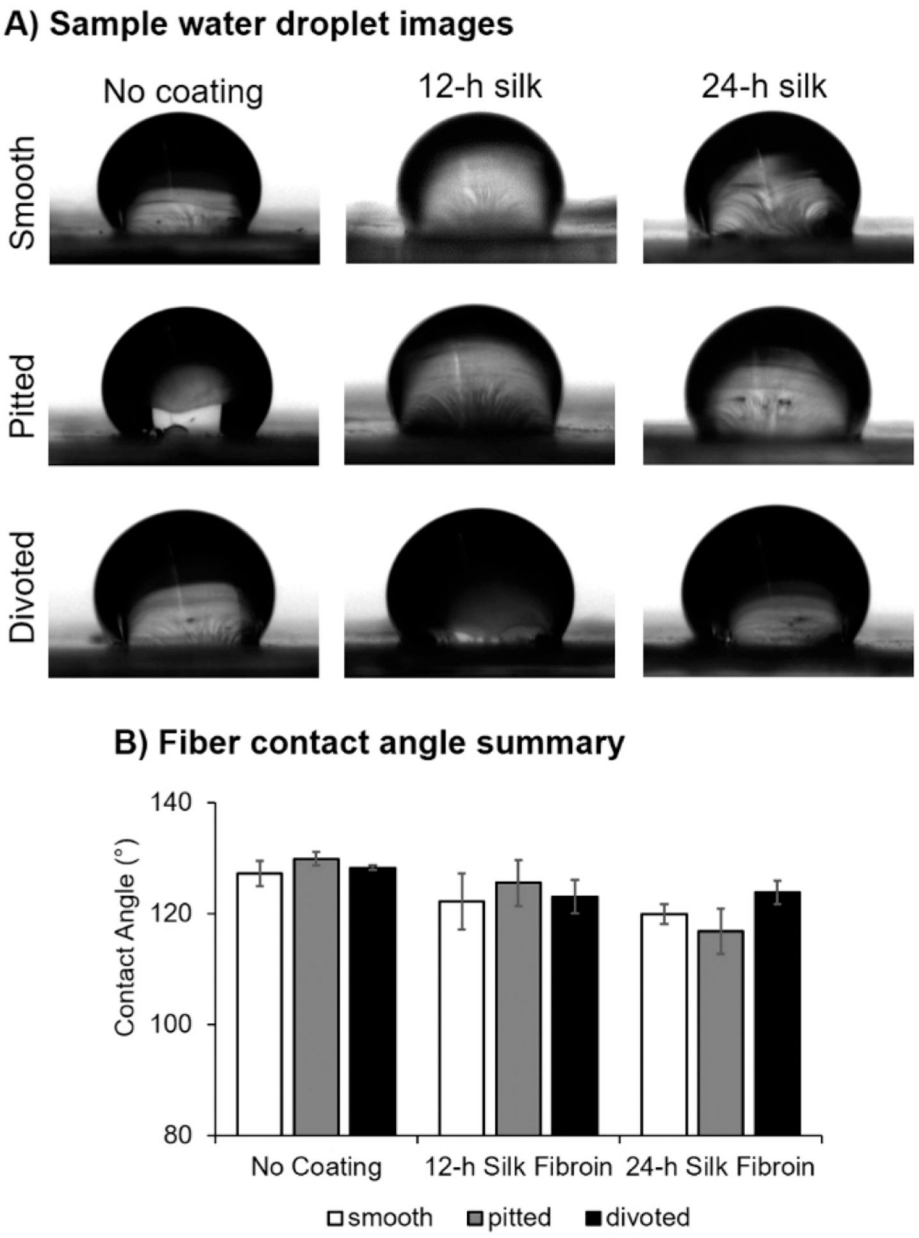


**Figure 3.**

Static water contact angle was unchanged after coating with SF. (A) Sample photographs of 3 $\mu$L water droplets applied to PLLA fibers. (B) Summary graph of average static contact angle on electrospun fibers. Data are shown as mean ± standard deviation. For summary data, $n = 3$ batches of fibers were assessed per group. Statistical significance between fiber groups was assessed using a Welch's ANOVA with post hoc Games–Howell test.

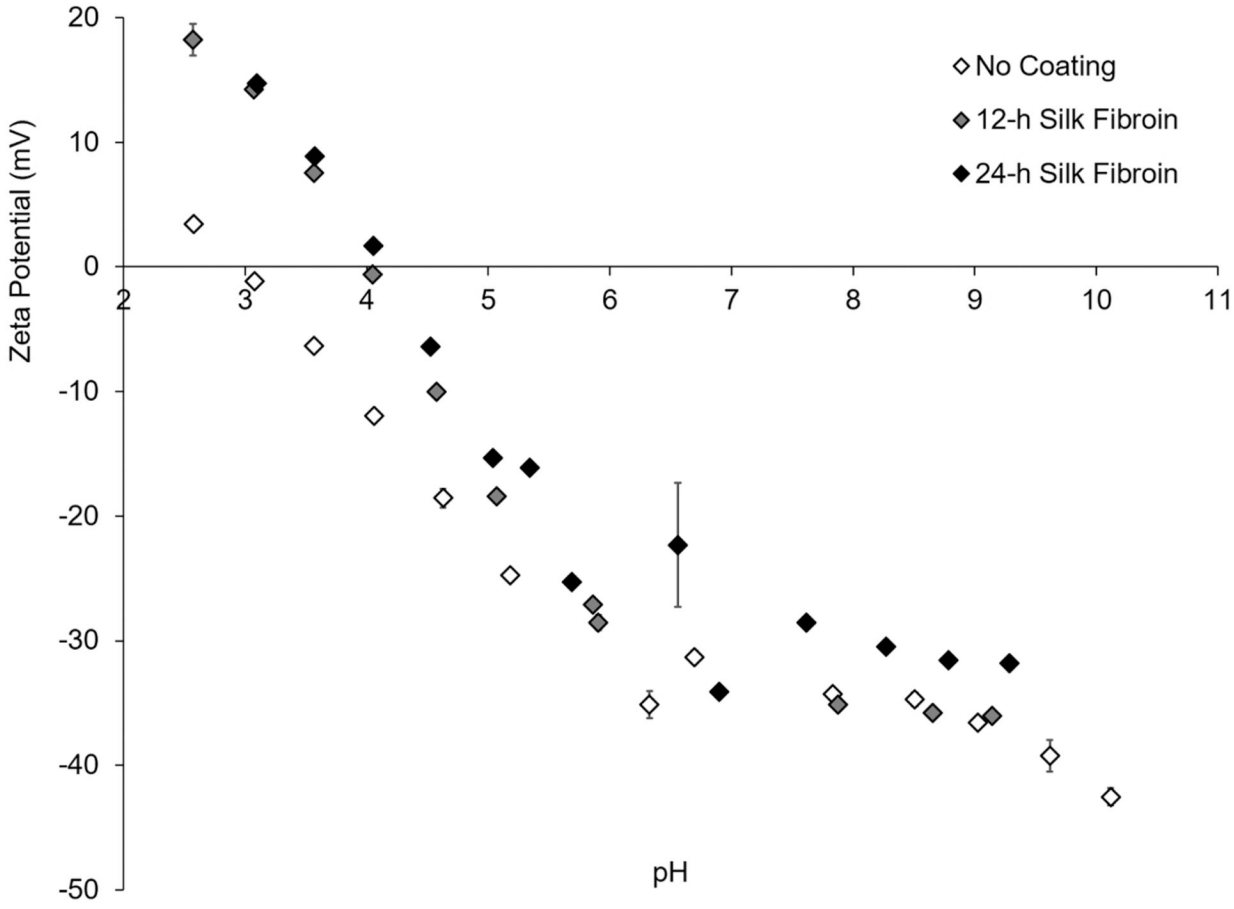


**Figure 4.**

ζ-potential measurements of SF-coated and uncoated PLLA films. ζ-potential values (mV) are very similar for coated and uncoated samples above a pH of 6 in 10 mM KCl, but there is a clear shift in the isoelectric point from 3 to 4 showing a change in surface chemistry due to the SF coating. Sample graph showing a single replicate ($n = 1$) of each coating condition, with 4 measurements taken at each pH between 2 and 10.

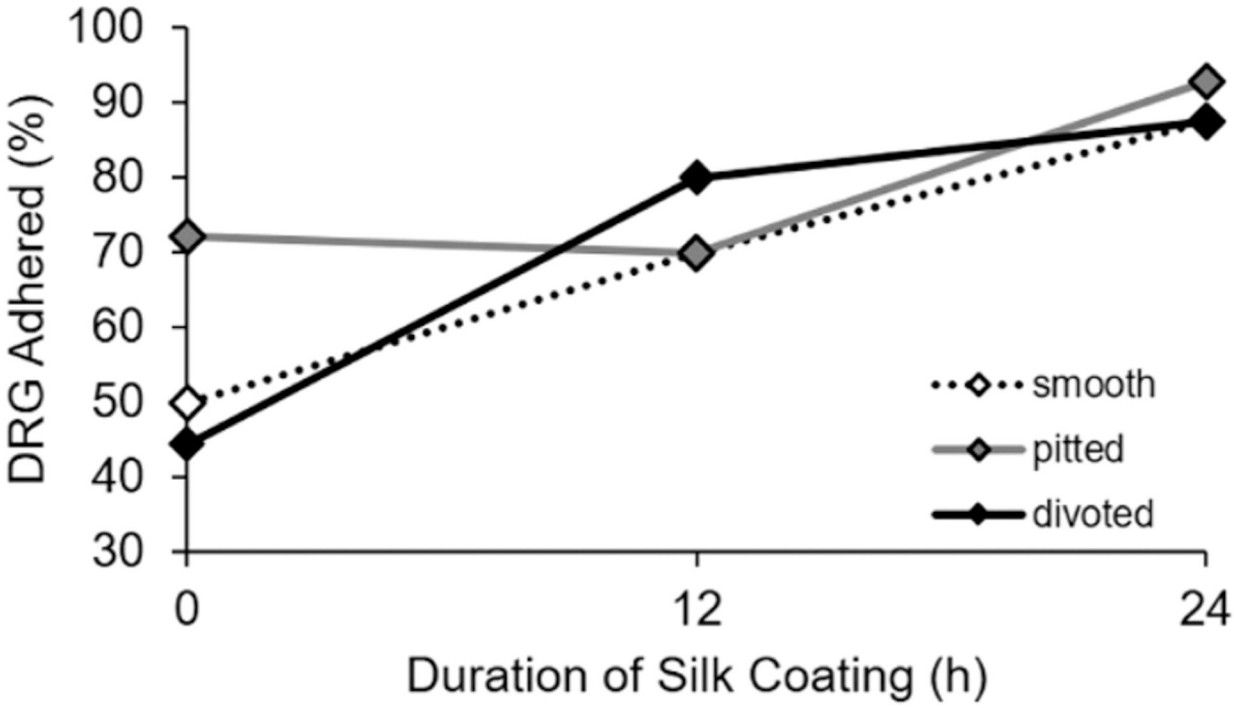


**Figure 5.**

Silk coatings enhance DRG adhesion on smooth and divoted fibers. The summary line plot displays the percentage of DRGs adhered on smooth, pitted, and divoted fibers that have no coating, a 12-h SF coating, or 24-h SF coating. A minimum of $n = 6$ DRG total from 4 separate animals were assessed per group. Statistically significant trends in adhesion were assessed using a binary logistic regression.

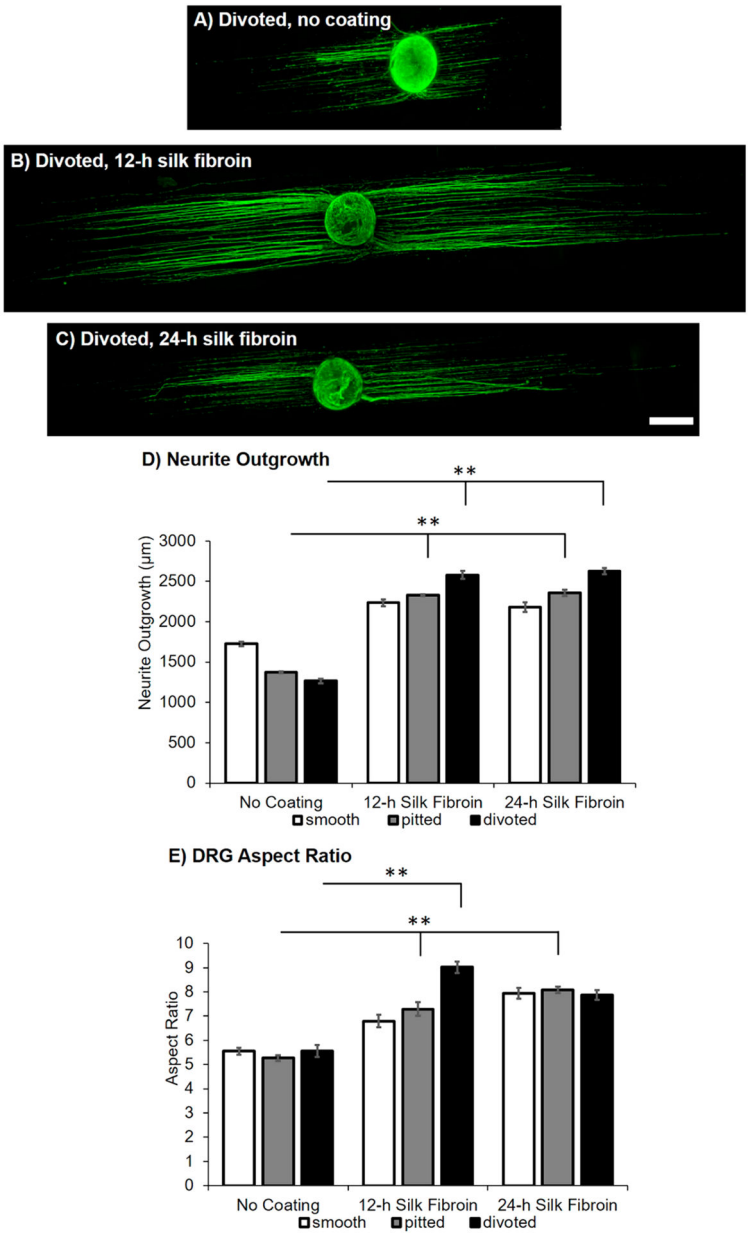


**Figure 6.**

Silk coatings increase neurite outgrowth on pitted and divoted fibers. Sample confocal microscopy images of immunostained DRG via neurofilament (green) on the following surfaces: (A) divoted, no coating, (B) divoted, 12-h coating, and (C) divoted, 24-h coating fiber surfaces (scale bar = 500 $\mu$m). (D) The summary graph displays the average neurite outgrowth for DRG cultured on smooth, pitted, and divoted fibers that have no coating, a 12-h SF coating, or 24-h SF coating. Data are shown as mean ± standard error of the mean. (E) The summary graph displays the aspect ratio (longest length/widest width) for DRG cultured on smooth, pitted, and divoted fibers that have no coating, a 12-h SF coating, or 24-h SF coating. Data are shown as mean ± standard error of the mean. A minimum of $n$ = 6 DRG from 4 separate animals were imaged for each fiber group. Statistical significance between

fiber groups for all analyses was assessed using a Welch's ANOVA with post hoc Games–Howell test (**$p < 0.001$).

**Table 1.**

Electrospinning Parameters for Electrospun PLLA Fibers Scaffolds

| fiber type | polymer in $CHCl_3$ (w/w %) | non-solvent in $CHCl_3$ (w/w %) | applied voltage (kV) | solution flow rate (mL/h) | mandrel rotation speed (RPM) | fiber collection distance (cm) | relative humidity during electrospinning (%) | fiber collection time (min) |
|---|---|---|---|---|---|---|---|---|
| smooth | 12 | N/A | 15 | 2.08 | 1000 | 5 | ≤21 | 10 |
| pitted | 12 | 1.80% DMSO | 15 | 2.08 | 1000 | 5 | 28–32 | 10 |
| divoted | 12 | N/A | 15 | 2.08 | 1000 | 5 | 28–32 | 10 |

*ACS Biomater Sci Eng*. Author manuscript; available in PMC 2021 July 13.

**Table 2.**

Mean ± Standard Deviation of pI Values for Drop Cast PLLA Films with SF Coatings[a]

| coating condition | pI |
|---|---|
| bare PLLA (no coating) | 2.96 ± 0.10 |
| 12-h silk fibroin | 4.01 ± 0.15[b] |
| 24-h silk fibroin | 3.94 ± 0.20[b] |

[a]Measurements were taken using $n = 3$ technical replicates of films with each coating.

[b]Significant increase in pI compared to no coating via a one-way ANOVA with post hoc Dunnett's Test ($p < 0.001$).